



Published in final edited form as:

*Bone*. 2007 October ; 41(4): 733–739.

## LOCATIONS OF BONE TISSUE AT HIGH RISK OF INITIAL FAILURE DURING COMPRESSIVE LOADING OF THE HUMAN VERTEBRAL BODY

Senthil K. Eswaran<sup>1</sup>, Atul Gupta<sup>1</sup>, and Tony M. Keaveny<sup>1,2</sup>

<sup>1</sup> *Orthopaedic Biomechanics Laboratory, Department of Mechanical Engineering, University of California, Berkeley, CA 94720, USA*

<sup>2</sup> *Department of Bioengineering, University of California, Berkeley, CA 94720, USA*

### Abstract

Knowledge of the location of initial regions of failure within the vertebra — cortical shell, cortical endplates vs. trabecular bone, as well as anatomic location — may lead to improved understanding of the mechanisms of aging, disease and treatment. The overall objective of this study was to identify the location of the bone tissue at highest risk of initial failure within the vertebral body when subjected to compressive loading. Toward this end, micro-CT based 60-micron voxel-sized, linearly elastic, finite element models of a cohort of thirteen elderly (age range: 54–87 years,  $75 \pm 9$  years) female whole vertebrae without posterior elements were virtually loaded in compression through a simulated disc. All bone tissue within each vertebra having either the maximum or minimum principal strain beyond its 90<sup>th</sup> percentile was defined as the tissue at highest risk of initial failure within that particular vertebral body. Our results showed that such high-risk tissue first occurred in the trabecular bone and that the largest proportion of the high-risk tissue also occurred in the trabecular bone. The amount of high-risk tissue was significantly greater in and adjacent to the cortical endplates than in the mid-transverse region. The amount of high-risk tissue in the cortical endplates was comparable to or greater than that in the cortical shell regardless of the assumed Poisson's ratio of the simulated disc. Our results provide new insight into the micromechanics of failure of trabecular and cortical bone within the human vertebra, and taken together, suggest that during strenuous compressive loading of the vertebra, the tissue near and including the endplates is at the highest risk of initial failure.

### Keywords

Vertebral body; Micromechanics; Initial failure; Trabecular bone; Cortical bone; Failure location

### Introduction

A fundamental issue in understanding the biomechanical failure mechanisms in osteoporotic vertebral fractures is the spatial distribution and location of tissue failure within the vertebral

---

Corresponding author: Senthil K. Eswaran, 2166 Etcheverry Hall, University of California, Berkeley, CA 94720-1740 USA, (510) 642-3787, fax (510) 642-6163, senthilk@me.berkeley.edu.

**Please address all reprint requests to:** Tony M. Keaveny, 6175 Etcheverry Hall, University of California, Berkeley, CA 94720-1740, USA, (510) 643-8017, fax (510) 642-6163, tmk@me.berkeley.edu

**Publisher's Disclaimer:** This is a PDF file of an unedited manuscript that has been accepted for publication. As a service to our customers we are providing this early version of the manuscript. The manuscript will undergo copyediting, typesetting, and review of the resulting proof before it is published in its final citable form. Please note that during the production process errors may be discovered which could affect the content, and all legal disclaimers that apply to the journal pertain.

body. Knowledge of the regions within the vertebra at highest risk of biomechanical failure — cortical shell, cortical endplates vs. trabecular bone as well as the anatomic locations — may lead to improved understanding of the mechanisms of aging, disease, and treatment. Identifying these high-risk regions may also provide insight into diagnosis of osteoporotic vertebral fractures, which remains a controversial topic [1]. Furthermore, possible differences in therapeutic effects of treatments on the cortical vs. trabecular bone [2] have led to renewed focus on the load-bearing role of the cortical shell and the relative importance of failure of cortical and trabecular bone.

Cadaver studies investigating the location of tissue failure within the vertebral body have so far been restricted to analysis of sagittal sections [3,4] because the three-dimensional nature of whole bone experiments obscures visualization of failure distributions. Bay *et al.* [4] used an image correlation technique to measure the strain distribution in sagittal sections of spinal segments under compressive loading and showed that strain concentrations developed in the trabecular bone adjacent to the superior cortical endplate and adjacent to the anterior cortex. Finite element computer modeling of whole vertebral bodies has been used to describe the tissue-level stress/strain spatial distributions within the whole vertebral body [5–7]. Several studies have demonstrated the ability of stress/strain distributions from finite element models to predict observed regions of failure [3,8]. While experiments [9] have shown that disc degeneration alters the loading conditions on the cortical endplates of the vertebral body, results from computational studies [10] suggest that the average effect of the altered loading conditions on vertebral strength may not be appreciable. High-resolution micro-CT based finite element modeling of whole vertebrae (40–60 micron voxel size) has enabled accurate characterization of the thin, porous shell and trabecular microarchitecture, and has helped resolve long-standing issues such as the substantial load-bearing role of the cortical shell [11,12]. Homminga *et al.* [6] compared a single normal vertebra to an osteoporotic vertebra and found that the osteoporotic vertebra was less resistant to “error” loads developed due to forward flexion or lifting. Despite the significant insight gained from these previous studies, the spatial distribution of failure and regions of failure initiation within the vertebral body remain poorly understood.

The overall goal of this study was to identify the location of bone tissue that is at highest risk of initial failure within the vertebral body when the vertebra is loaded in compression. Toward this end, high-resolution micro-CT-based finite element models were analyzed for a cohort of elderly cadaver vertebrae to quantify the strain distribution throughout the vertebral body. Our specific objectives were to: 1) determine whether the bone tissue at high risk of failure first occurs in the trabecular bone, cortical shell, or cortical endplates by quantifying the relative amount of high-risk tissue in each unit; 2) identify the anatomical location (inferior/superior) of such high-risk tissue; and 3) determine the sensitivity of these results to how the endplate is loaded, i.e. via a disc or a layer of PMMA, the latter often used in biomechanical testing of isolated vertebrae [13–15]. This study is the first to use such detailed analysis techniques to describe the micromechanics of initial failure at the tissue level in a cohort of elderly human vertebrae.

## Materials and Methods

Thirteen T10 whole vertebral bodies were obtained from female human cadavers (age range: 54–87 years,  $74.6 \pm 9.4$  years) with no medical history of metabolic bone disorders. These specimens were analyzed previously to understand the load sharing between cortical and trabecular bone [11]. Briefly, the posterior elements were removed, the vertebrae were micro-CT scanned at 30  $\mu\text{m}$  voxel size (Scanco 80, Scanco Medical AG, Basserdorf, Switzerland), rotated to a vertical orientation, region-averaged to 60  $\mu\text{m}$  voxel size and then thresholded using a global threshold value. A voxel size of 60  $\mu\text{m}$  was chosen based on a detailed

convergence study (Appendix A) which showed that the error associated with the 60- $\mu\text{m}$  model was minimal for the outcome variable of interest in this study. An averaging technique [11, 12] was used within an image processing software (IDL, Research Systems Inc., Boulder, CO) to identify the cortical shell and cortical endplates. Since it was difficult to clearly identify the transition from the endplate to the cortical shell, the bone tissue at the corner regions were also tagged with a unique identifier (Figure 1). Each 60  $\mu\text{m}$  cubic voxel was then converted into an 8-noded finite element to create a finite element model of the entire vertebral body (without posterior elements). The trabecular microarchitectural parameters — trabecular bone volume fraction (BV/TV), trabecular thickness (Tb. Th.), trabecular spacing (Tb. Sp.) and structural model index (SMI) were calculated (Skyscan: CTAn software) using the 60-micron models (Table 1). The average thickness of the cortical shell was determined in the region excluding the cortical endplates [11].

All bone tissue was assigned the same hard tissue properties (elastic modulus of 18.5 GPa and Poisson's ratio of 0.3) since the cortical shell is often described as condensed trabeculae [16–18]. The disc was assumed to be degenerated since the mean age of the cadaver specimens was 75 years. The disc (of height 5 mm [19]) was modeled using symmetry boundary conditions at its mid-transverse plane. Thus, a disc of height 2.5 mm was added to the superior and inferior endplates of the vertebral body. Based on evidence from the literature that the degenerated nucleus pulposus loses its fluid-like behavior [20,21], the disc (on both superior and inferior sides) was modeled as a homogeneous elastic isotropic material having properties typical of the annulus (compressive elastic modulus of 8 MPa [22] and Poisson's ratio of 0.45 [23,24]). In order to test the sensitivity of our results to the assumed material properties of the disc, a second set of analyses were run using a Poisson's ratio of 0.3 for the disc. A previous parametric study had indicated that the load sharing between the cortical shell and trabecular bone was insensitive to the assumed modulus of the disc [11], and therefore, the focus here was specifically on the sensitivity of our results to the assumed Poisson's ratio of the disc. Further, to simulate a common biomechanical test on isolated vertebra [13–15], a third set of analyses were run in which the vertebral body was loaded through a PMMA layer (Young's modulus of 2500 MPa and Poisson's ratio of 0.3 [25]) instead of a disc.

Depending on the vertebra size, the resulting finite element models had up to 60 million elements and 220 million degrees of freedom and required specialized software and hardware for analysis. All analyses were run on an IBM Power4 supercomputer (IBM corporation, Armonk, NY) using a maximum of 440 processors in parallel and 900 GB memory, and a custom code with a parallel mesh partitioner and algebraic multigrid solver [26], requiring a total of approximately 4300 CPU hours. To simulate compressive loading of each vertebra, an apparent level compressive strain of 1.0% was applied to each model by using different displacement magnitudes based on the height of each model. The top surface of each model was displaced in the superior-inferior direction using roller-type boundary conditions applied at the mid-plane of the disc/PMMA layer, while the bottom surface was fixed using minimal frictionless constraints to prevent rigid body motion.

A number of outcome parameters were used to identify the bone tissue at highest risk of initial failure. The 90<sup>th</sup> percentiles of the tissue-level maximum and minimum principal strains were calculated at an apparent level strain of 1.0% for each vertebral body (Table 2). Any bone element having either its maximum or minimum principal strain beyond the corresponding 90<sup>th</sup> percentile was identified as “high-risk tissue”. For example, for specimen #1, a bone element having its maximum principal strain (400  $\mu\text{strain}$ ) beyond the 90<sup>th</sup> percentile of the maximum principal strain for that vertebra (347  $\mu\text{strain}$ ), or a bone element having its minimum principal strain (–450  $\mu\text{strain}$ ) beyond the 90<sup>th</sup> percentile of the minimum principal strain for that vertebra (–430  $\mu\text{strain}$ ) would be identified as high-risk tissue. Since tissue-level stress/strain distributions from linear finite element models have correlated well with observed

microdamage [8] and since regions experiencing high strain are likely to fail first, the high-risk tissue identified in this study represents the bone tissue at highest risk of *initial* failure within that particular vertebral body. This approach facilitates comparison across multiple vertebrae exhibiting considerable heterogeneity in their strain distributions (Table 2) since the amount of high-risk tissue in each vertebra was similar by design. Moreover, using the percentiles approach ensured that the results reported here are independent of the choice of the applied apparent level strain. The relative amount of high-risk tissue at an apparent strain of 1.0% was calculated as the amount of high-risk tissue in a particular unit (trabecular bone, cortical shell, cortical endplates, or corner) with respect to the total amount of high-risk tissue in the vertebral body at an apparent strain of 1.0%. The variation of the amount of high-risk tissue across transverse or coronal slices of each vertebral body was also determined at an applied apparent strain of 1.0%.

A linear scaling of the tissue-level principal strains was used to predict the dependence of the amount of high-risk tissue on the magnitude of the applied apparent strain. The purpose of this analysis was to determine whether high-risk tissue first occurred in the trabecular bone, cortical shell or endplates. As with previous outcome measures, this result is independent of the absolute value of the applied apparent level strain. In particular, for each element identified to be at high-risk at 1.0% apparent strain, the applied apparent strain on the whole vertebral body at which that element would first exceed the 90<sup>th</sup> percentile was determined by linear scaling. For example, at an applied apparent strain of 1.0%, if the 90<sup>th</sup> percentile of the maximum principal strain was 300  $\mu$ strain and the maximum principal strain of a particular element was 400  $\mu$ strain, then this high-risk element would first exceed the 90<sup>th</sup> percentile at an apparent strain of 0.75%. The relative amount of high-risk tissue in the different units — trabecular bone, cortical shell, cortical endplates and corner regions — at apparent level strain increments of 0.05% was calculated as the amount of high-risk tissue belonging to a particular unit at that apparent strain divided by the total amount of high-risk tissue identified at 1.0% apparent level strain. The relative amounts of high-risk tissue in the trabecular and cortical bone were then compared at each apparent level strain increment using a paired Student's t-test with Bonferroni adjustment for multiple comparisons.

## Results

Across all vertebrae, high-risk tissue, i.e. tissue loaded beyond the 90<sup>th</sup> percentile within each vertebral body, first occurred in the trabecular bone (Figure 2). Trabecular bone had significantly more high-risk tissue as compared to cortical bone when the applied apparent strain was greater than 0.3% ( $p < 0.05$ ). At an applied apparent level strain of 1.0%, an average (mean  $\pm$  S.D.) of  $53.7\% \pm 5.5\%$  of the high-risk tissue was in the trabecular bone, which was significantly greater ( $p < 0.0001$ ) than the relative amount of high-risk tissue in the cortical endplates ( $19.5 \pm 2.3\%$ ), corner regions ( $16.3 \pm 5.0\%$ ), and the cortical shell ( $10.4 \pm 2.7\%$ ).

Regarding the anatomic location of initial failure, the amount of high-risk tissue in and adjacent to the cortical endplates was significantly greater than in the mid-transverse region (Figure 3A, 3B). The amount of high-risk trabecular tissue was also significantly greater near the cortical endplates than in the mid-transverse region (Figure 3C) and there was a concentration of high-risk tissue in the cortical endplates (Figure 3A, 4).

The amount of high-risk tissue in the cortical endplates was comparable to or greater than that in the cortical shell regardless of the assumed Poisson's ratio of the simulated disc (Figure 5). By contrast, for loading the vertebral body through a PMMA layer, there was a complete absence of high-risk tissue in the cortical endplates (Figures 4, 5). The amount of high-risk tissue within the cortical endplates decreased from  $19.5\% (\pm 2.3\%)$  to  $12.6\% (\pm 3.3\%)$  when

the Poisson's ratio of the disc was reduced from 0.45 to 0.30 (Figure 5); the respective measures for the amount of high-risk tissue in the cortical shell were 10.4% ( $\pm 2.7\%$ ) and 13.2% ( $\pm 2.6\%$ ).

## Discussion

The overall goal of this study was to identify the location of the bone tissue at highest risk of initial failure within the vertebral body for uniform compressive loading of the vertebra. Our results showed for these loading conditions that high-risk tissue first occurred in the trabecular bone and that the largest proportion of high-risk bone tissue was in the trabecular bone. The amount of high-risk tissue in the trabecular bone was least at the mid-transverse section (Figure 3C). This finding is consistent with previous studies which have shown that the trabecular bone takes minimum load around the mid-transverse section of the vertebral body as a result of the load sharing between trabecular bone and cortical shell [5, 11]. Although the inferior-superior location of the high-risk tissue in the cortical shell followed an opposing trend to that of the trabecular bone, the total amount of high-risk tissue was greater in and adjacent to the cortical endplates compared to the mid-transverse region. The amount of high-risk bone tissue in the cortical endplates was comparable to or greater than that in the cortical shell regardless of the disc properties assumed. Taken together, these results suggest that, during strenuous compressive loading of the vertebra, the tissue in and adjacent to the endplates is at highest risk of initial failure.

One notable feature of this study was our analysis of multiple vertebral bodies. This enabled us to provide statistical estimates of variances for each outcome variable and also afforded the study a reasonable degree of external validity. In addition, each vertebral body was compartmentalized into trabecular bone, cortical shell and cortical endplates using a previously verified algorithm [11], thereby providing unique insight into the relative failure behavior between these units. Parametric studies were performed to assess the sensitivity of our results to how the disc was modeled. Using the 90<sup>th</sup> percentile approach ensured that our results were independent of the choice of the applied apparent level strain, provided a normalized setting for comparing initial failure variations across multiple vertebrae and circumvented the need to model actual failure, which is a computationally prohibitive problem for multiple whole vertebrae at this juncture. While this approach is not ideal for absolute tissue-level failure predictions, it should provide valid comparative results for integrated outcomes such as locations of initial failure, variations in initial failure across transverse slices, and the relative amount of initial failure in cortical vs. trabecular bone.

The main caveat of this study was that the loading mode used in all analyses was uniform compression. Since most osteoporotic vertebral fractures are wedge fractures [27], the response to forward flexion loading is of clinical interest. The *in vivo* loads that are imparted to the vertebral body during forward flexion are not well understood, particularly the magnitude of any bending moment applied to the vertebral body. Recent work by Adams and co-workers [28,29] showed that when motion segments were compressed in a flexed posture, the posterior elements had little structural role (<10% of the overall load), presumably because the facet joints are open for such loading. In this study, we simulated such loading conditions in part by removing the posterior elements. The other aspect of simulating forward flexion, i.e., the amount of any added bending moment experienced by the vertebra compared to what develops for uniform compression, remains unclear and was not included in the model. The cortical shell may play a more important role if the vertebral body is subjected to large additional bending moments during forward flexion since peripheral bone is thought to have a greater structural role when the vertebra is forced to bend [30]. Further work is required to address this issue.

A second caveat was that our results describe regions of initial failure, which are not necessarily the regions of final failure. The consistency of our results with those from a single fully

nonlinear analysis (Appendix B, Figure 6) supports the validity of our approach to identifying the regions in which the tissue is most likely to fail initially. However, these analyses did not capture the nonlinearities that may influence the subsequent failure behavior of the vertebral body such as localized large deformation effects [31–33]. In theory, individual trabeculae may fail by buckling although they may not be the most highly-strained trabeculae, especially if they are long and slender [32, 34]. Thus, regions of initial failure, as described here, may not correspond with all regions of subsequent failure and fully nonlinear analyses are required to resolve this issue.

Another potential limitation was that the intervertebral disc was modeled as a homogeneous elastic isotropic material when in fact its material behavior is more complex [22,35]. Based on existing literature that the degenerated nucleus pulposus has a solid-like behavior [20,21], we assigned annulus-type material properties to the entire disc. This simulated a state of degeneration associated with the aged nature of the vertebrae used in this study and perhaps has more direct clinical relevance to osteoporosis than if a more fluid-like healthy disc were simulated. Our sensitivity analysis to the assumed value of the Poisson's ratio of the disc indicated that the amount of high-risk tissue in the cortical endplates was reduced as Poisson's ratio was decreased. This suggests that modeling the intervertebral disc as a heterogeneous structure may potentially affect the location and amount of high-risk tissue at the cortical endplates. However, regardless of the assumed value of the Poisson's ratio, there was tensile stretching and bending of the cortical endplates associated with the lateral expansion of the simulated disc. This resulted in the cortical endplates being highly strained, predominantly in transverse tension despite the overall axial compressive loading. By contrast, this tension in the endplates completely disappeared when the disc was replaced with PMMA. Given the similarity of the results for the different disc models and the large difference versus the PMMA model, it is unlikely that the general trends reported here would be altered appreciably if we had modeled the degenerated disc using a more complex constitutive model.

Consistent with previous experiments [4,9], our results show that high-risk tissue first occurred in the trabecular bone and that there was more high-risk tissue near and including the cortical endplates compared to the mid-transverse region. Specifically, a previous experimental cadaver study [4] which analyzed sagittal sections of the vertebral body using texture analysis found that the superior endplate region adjacent to the nucleus pulposus remained the most highly strained region throughout the loading cycle, consistent with our results. That study also found a second region of high strain magnitude adjacent to the mid-anterior cortex — not observed in this study — at loads greater than 60% of the failure load of the vertebral section. The discrepancy could be because our results (based on linear analyses) pertain only to initial failure and hence, are not necessarily those associated with the final collapse of the vertebral body. Our finding of a large amount of high-risk tissue in the trabecular bone is consistent with previous laboratory observations that the damage behavior of the whole vertebral body is dominated by that of the trabecular bone [14]. The high-risk regions observed at the cortical endplates is also consistent with recent clinical observations [1] that radiological evidence of changes in the endplate may be an essential part of the definition of a vertebral fracture. Though the current study was limited to the T10 vertebral level — which has lower fracture incidence compared to other levels such as T8 or L1 [36] — the consistency of our results with previous studies on thoracolumbar vertebrae [4,9] suggests that the tissue in and adjacent to the cortical endplates is involved in the initial failure of thoracolumbar vertebra in general. Finally, our finding that initial failure occurs throughout the vertebra further strengthens the gathering evidence in the literature [11,37,38] that an integrative approach to analyzing the entire vertebral body — by incorporating trabecular bone, cortical endplates and cortical shell — may improve the clinical assessment of aging, disease, and treatment on vertebral strength.

## Acknowledgements

Funding was provided by National Institute of Health grant AR49828. Computational resources were available through grant UCB-254 and UCB-266 from the National Partnership for Computational Infrastructure. All the finite element analyses were performed on an IBM Power4 supercomputer (Datastar, San Diego Supercomputer Center). Human tissue was obtained from National Disease Research Interchange and the University of California at San Francisco. Micro-CT scanning was performed at Exponent Inc., Philadelphia. We would like to thank SkyScan, Belgium for providing the CTAn software. Dr. Keaveny has a financial interest in O.N. Diagnostics and both he and the company may benefit from the results of this research.

## References

1. Ferrar L, Jiang G, Adams J, Eastell R. Identification of vertebral fractures: an update. *Osteoporos Int* 2005;16(7):717–28. [PubMed: 15868071]
2. Black DM, Greenspan SL, Ensrud KE, Palermo L, McGowan JA, Lang TF, et al. The effects of parathyroid hormone and alendronate alone or in combination in postmenopausal osteoporosis. *N Engl J Med* 2003;349(13):1207–15. [PubMed: 14500804]
3. Silva MJ, Keaveny TM, Hayes WC. Computed tomography-based finite element analysis predicts failure loads and fracture patterns for vertebral sections. *Journal of Orthopaedic Research* 1998;16:300–308. [PubMed: 9671924]
4. Bay BK, Yerby SA, McLain RF, Toh E. Measurement of strain distributions within vertebral body sections by texture correlation. *Spine* 1999;24(1):10–17. [PubMed: 9921585]
5. Homminga J, Weinans H, Gowin W, Felsenberg D, Huiskes R. Osteoporosis changes the amount of vertebral trabecular bone at risk of fracture but not the vertebral load distribution. *Spine* 2001;26(14):1555–61. [PubMed: 11462085]
6. Homminga J, Van-Rietbergen B, Lochmuller EM, Weinans H, Eckstein F, Huiskes R. The osteoporotic vertebral structure is well adapted to the loads of daily life, but not to infrequent “error” loads. *Bone* 2004;34(3):510–6. [PubMed: 15003798]
7. Shirazi-Adl SA, Shrivastava SC, Ahmed AM. Stress analysis of the lumbar disc-body unit in compression: A three-dimensional nonlinear finite element study. *Spine* 1984;9(2):120–134. [PubMed: 6233710]
8. Nagaraja S, Couse TL, Guldberg RE. Trabecular bone microdamage and microstructural stresses under uniaxial compression. *Journal of Biomechanics* 2005;38(4):707–716. [PubMed: 15713291]
9. Hansson T, Roos B. The Relation between Bone-Mineral Content, Experimental Compression Fractures, and Disk Degeneration in Lumbar Vertebrae. *Spine* 1981;6(2):147–153. [PubMed: 7280815]
10. Buckley JM, Leang DC, Keaveny TM. Sensitivity of vertebral compressive strength to endplate loading distribution. *J Biomech Eng* 2006;128(5):641–6. [PubMed: 16995749]
11. Eswaran SK, Gupta A, Adams MF, Keaveny TM. Cortical and trabecular load sharing in the human vertebral body. *Journal of Bone and Mineral Research* 2006;21(2):307–314. [PubMed: 16418787]
12. Eswaran SK, Bayraktar HH, Adams MF, Gupta A, Hoffman PF, Lee DC, et al. The micromechanics of cortical shell removal in the human vertebral body. *Computer Methods in Applied Mechanics and Engineering*. 2006Accepted
13. Eriksson SAV, Isberg BO, Lindgren JU. Prediction of Vertebral Strength by Dual Photon-Absorptiometry and Quantitative Computed-Tomography. *Calcified Tissue International* 1989;44(4):243–250. [PubMed: 2501006]
14. Kopperdahl DL, Pearlman JL, Keaveny TM. Biomechanical consequences of an isolated overload on the human vertebral body. *Journal of Orthopaedic Research* 2000;18:685–690. [PubMed: 11117287]
15. Faulkner KG, Cann CE, Hasegawa BH. Effect of bone distribution on vertebral strength: assessment with patient-specific nonlinear finite element analysis. *Radiology* 1991;179(3):669–74. [PubMed: 2027972]
16. Silva MJ, Wang C, Keaveny TM, Hayes WC. Direct and Computed-Tomography Thickness Measurements of the Human, Lumbar Vertebral Shell and End-Plate. *Bone* 1994;15(4):409–414. [PubMed: 7917579]

17. Roy ME, Rho JY, Tsui TY, Evans ND, Pharr GM. Mechanical and morphological variation of the human lumbar vertebral cortical and trabecular bone. *Journal of Biomedical Materials Research* 1999;44(2):191–197. [PubMed: 10397920]
18. Mosekilde L. Vertebral Structure and Strength in-Vivo and in-Vitro. *Calcified Tissue International* 1993;53:S121–S126. [PubMed: 8275365]
19. Oliver, J.; Middleditch, A. *Functional anatomy of the spine*. Boston, MA: Butterworth-Heinemann; 1991. p. 62-64.
20. Iatridis JC, Setton LA, Weidenbaum M, Mow VC. Alterations in the mechanical behavior of the human lumbar nucleus pulposus with degeneration and aging. *J Orthop Res* 1997;15(2):318–22. [PubMed: 9167638]
21. Bernick S, Walker JM, Paule WJ. Age changes to the anulus fibrosus in human intervertebral discs. *Spine* 1991;16(5):520–4. [PubMed: 1711242]
22. Duncan, NA.; Lotz, JC. Experimental validation of a porohyperelastic finite element model of the annulus fibrosus. In: Pande, GN., editor. *Computer Methods in Biomechanics and Biomedical Engineering*. Amsterdam, Netherlands: Gordon and Breach; 1998. p. 527-534.
23. Liu YK, Ray G, Hirsch C. The resistance of the lumbar spine to direct shear. *Orthop Clin North Am* 1975;6(1):33–49. [PubMed: 1113979]
24. Fagan MJ, Julian S, Siddall DJ, Mohsen AM. Patient-specific spine models. Part 1: finite element analysis of the lumbar intervertebral disc - a material sensitivity study *Proceedings of the Institution of Mechanical Engineers Part H. Journal of Engineering in Medicine* 2002;216(H5):299–314. [PubMed: 12365788]
25. Lewis G. Properties of acrylic bone cement: state of the art review. *J Biomed Mater Res* 1997;38(2): 155–82. [PubMed: 9178743]
26. Adams, MF.; Bayraktar, HH.; Keaveny, TM.; Papadopoulos, P. Ultrascale implicit finite element analyses in solid mechanics with over a half a billion degrees of freedom. *ACM/IEEE Proceedings of SC2004: High Performance Networking and Computing*; Pittsburg, PA, USA. 2004.
27. Eastell R, Cedel SL, Wahner HW, Riggs BL, Melton LJ. Classification of vertebral fractures. *Journal of Bone and Mineral Research* 1991;6(3):207–215. [PubMed: 2035348]
28. Pollintine P, Dolan P, Tobias JH, Adams MA. Intervertebral disc degeneration can lead to “stress-shielding” of the anterior vertebral body: a cause of osteoporotic vertebral fracture? *Spine* 2004;29(7):774–82. [PubMed: 15087801]
29. Adams MA, Pollintine P, Tobias JH, Wakley GK, Dolan P. Intervertebral disc degeneration can predispose to anterior vertebral fractures in the thoracolumbar spine. *J Bone Miner Res* 2006;21(9): 1409–16. [PubMed: 16939399]
30. Crawford RP, Keaveny TM. Relationship between axial and bending behaviors of the human thoracolumbar vertebra. *Spine* 2004;29(20):2248–55. [PubMed: 15480136]
31. Bevil G, Eswaran SK, Gupta A, Papadopoulos P, Keaveny TM. Influence of bone volume fraction and architecture on computed large-deformation failure mechanisms in human trabecular bone. *Bone* 2006;39(6):1218–25. [PubMed: 16904959]
32. Stolken JS, Kinney JH. On the importance of geometric nonlinearity in finite-element simulations of trabecular bone failure. *Bone* 2003;33(4):494–504. [PubMed: 14555252]
33. Muller R, Gerber SC, Hayes WC. Micro-compression: a novel technique for the nondestructive assessment of local bone failure. *Technol Health Care* 1998;6(5–6):433–44. [PubMed: 10100946]
34. Gibson LJ. The mechanical behavior of cancellous bone. *Journal of Biomechanics* 1985;18(5):317–328. [PubMed: 4008502]
35. Iatridis JC, Weidenbaum M, Setton LA, Mow VC. Is the nucleus pulposus a solid or a fluid? Mechanical behaviors of the nucleus pulposus of the human intervertebral disc. *Spine* 1996;21(10): 1174–84. [PubMed: 8727192]
36. Cooper C, Atkinson EJ, O’Fallon WM, Melton LJ. Incidence of clinically diagnosed vertebral fractures: a population-based study in Rochester, Minnesota, 1985–1989. *Journal of Bone and Mineral Research* 1992;7:221–227. [PubMed: 1570766]
37. Crawford RP, Cann CE, Keaveny TM. Finite element models predict in vitro vertebral body compressive strength better than quantitative computed tomography. *Bone* 2003;33(4):744–50. [PubMed: 14555280]

38. Andresen R, Werner HJ, Schober HC. Contribution of the cortical shell of vertebrae to mechanical behaviour of the lumbar vertebrae with implications for predicting fracture risk. *British Journal of Radiology* 1998;71(847):759–65. [PubMed: 9771387]

## Appendix A

A numerical convergence analysis was done to choose the appropriate voxel size based on a compromise between the computational expense involved and resulting error. For four specimens ( $BV/TV = 0.083 \pm 0.008$ ), mid-coronal 3-mm-thick vertebral slices (created using 30-micron and 60-micron voxel sizes) were subjected to compressive loading via a PMMA layer with plane-strain boundary conditions. The amount of high-risk tissue was identified in each model using the 90<sup>th</sup> percentile principal strain criterion. The variation in the amount of high-risk tissue across transverse slices predicted by the 60- $\mu\text{m}$  models compared favorably with that predicted by the 30-micron models. The mean difference in the amount of high-risk tissue at a transverse slice predicted by the 60- $\mu\text{m}$  and 30- $\mu\text{m}$  models (averaged across transverse slices of four specimens) was only  $-0.0004\%$  ( $\pm 0.003\%$ ) and was substantially lower than the mean amount of high-risk tissue at a transverse slice ( $0.035 \pm 0.018\%$ ).

## Appendix B

In order to help validate the use of linear finite element analyses for our outcomes, the results from the analysis of one vertebral body when loaded via a PMMA layer was compared with the results from a fully nonlinear analysis — including geometric and material nonlinearities [31]. Previously calibrated tissue-level yield strains — tensile and compressive yield strains of 0.33% and 0.81%, respectively [31] — were used in the nonlinear analysis which required approximately 15,000 CPU hours on a supercomputer. Results indicated that the relative distribution of the high-risk/failed bone tissue among the different units compared well between the linear and nonlinear analyses (Figure 6).

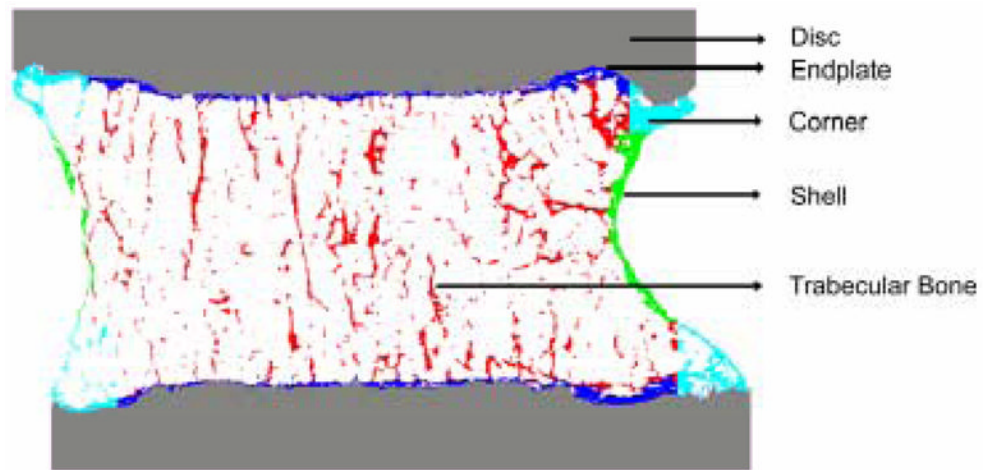


**Figure 1.** Sagittal slice (60-micron thick) of a vertebral body showing the different regions identified – trabecular bone (red), cortical shell (green), cortical endplates (dark blue), corner regions (cyan), and disc (gray).

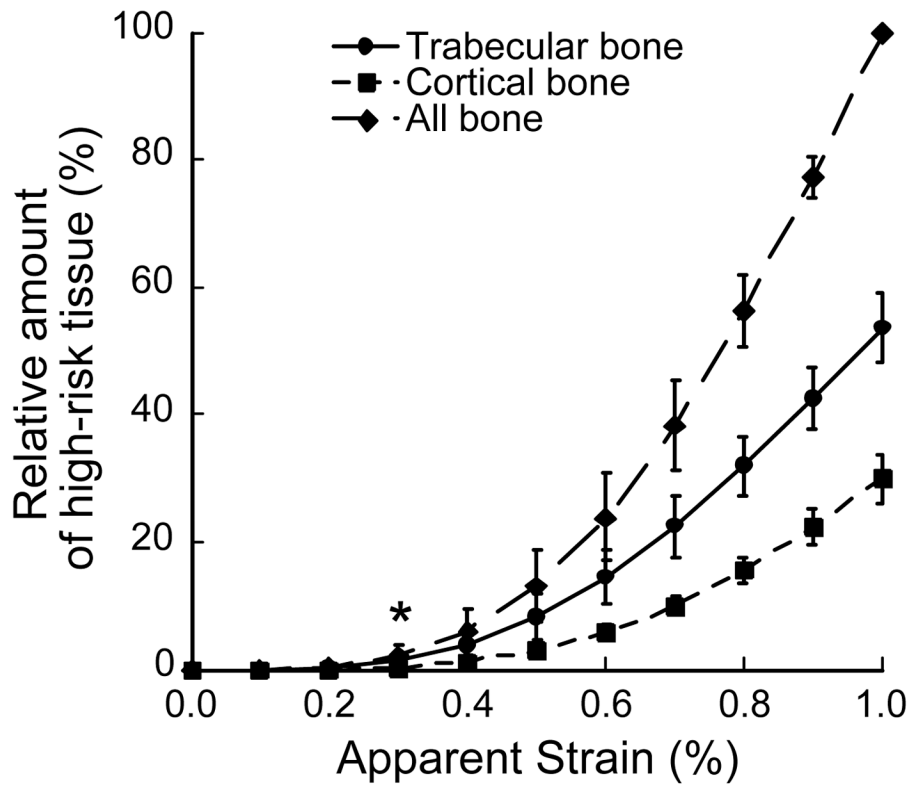


**Figure 2.**

Dependence of the relative amount of high-risk tissue on the magnitude of the apparent strain showing that the high-risk tissue first occurred in the trabecular bone. The relative amount of high-risk tissue at each apparent strain represents the amount of high-risk tissue belonging to a particular compartment at that strain divided by the total amount of high-risk tissue identified at 1.0% apparent level strain. Corner regions data were omitted from the plot for clarity. The disc was modeled using a Poisson's ratio of 0.45. Data presented in increments of 0.1% apparent level strain. Bars show SD for n=13 specimens.

\* Trabecular bone significantly different from cortical bone at all apparent strains above 0.3% ( $p < 0.05$ )

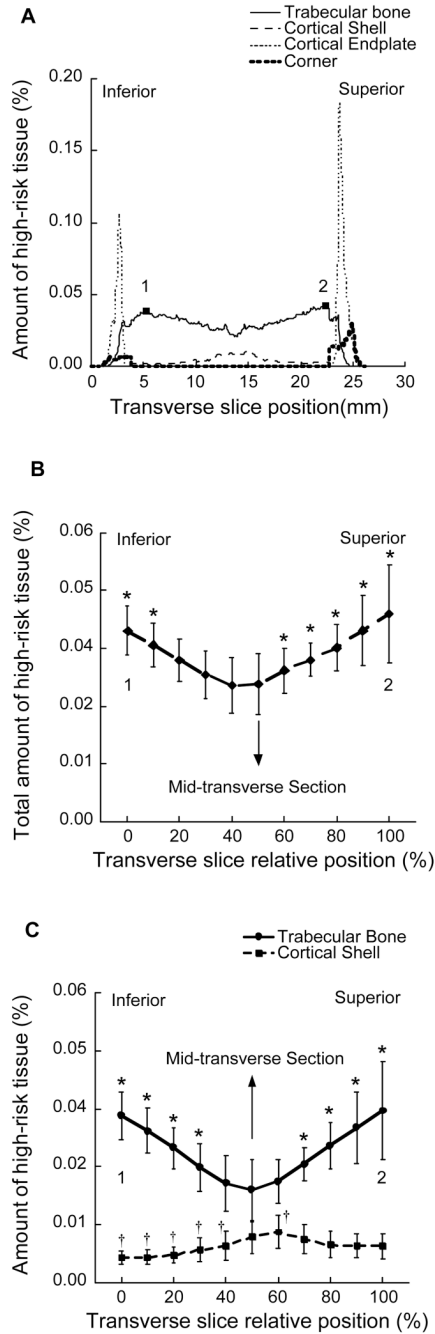


**Figure 3.**

**A:** Typical variation of the amount of high-risk tissue across transverse slices for one vertebra. **B:** Mean variation in the total amount of high-risk tissue across transverse slices in the region excluding the cortical endplates (between points 1–2, Figure 3A), showing that there was more high-risk tissue adjacent to the cortical endplates than in the middle region. Bars show SD for n=13 specimens. **C:** Mean variation of the amount of high-risk tissue in the trabecular bone and cortical shell in the region excluding the endplates. Transverse slice relative position indicates the relative distance between positions 1 and 2 identified in Figure 3A. All results presented at an apparent level strain of 1.0%.

\* Amount of high-risk tissue at these transverse slice positions was significantly different from that at the mid-transverse section ( $p < 0.05$ )

† Amount of high-risk tissue in the cortical shell tissue at these transverse slices was significantly different from that at the mid-transverse section ( $p < 0.05$ ).

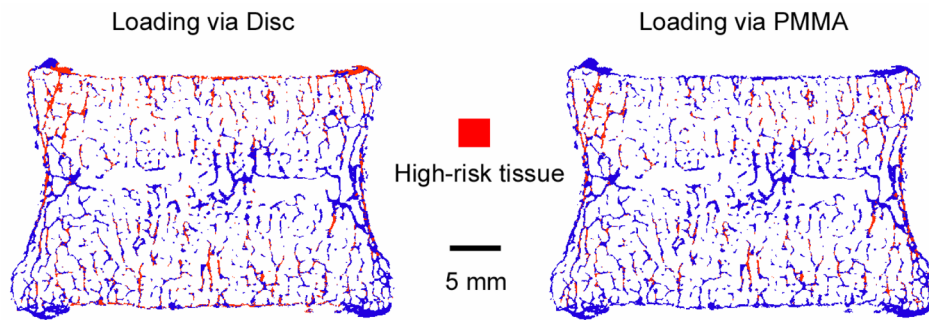


**Figure 4.** Distribution of high-risk tissue (red) at the mid-coronal slice of a vertebral body when loaded via a simulated disc (Left, Poisson's ratio of 0.45) illustrating that there was more high-risk tissue in and adjacent to the cortical endplates than near the middle region. Loading via a PMMA layer (Right) led to a protection of the cortical endplates which were no longer highly strained.

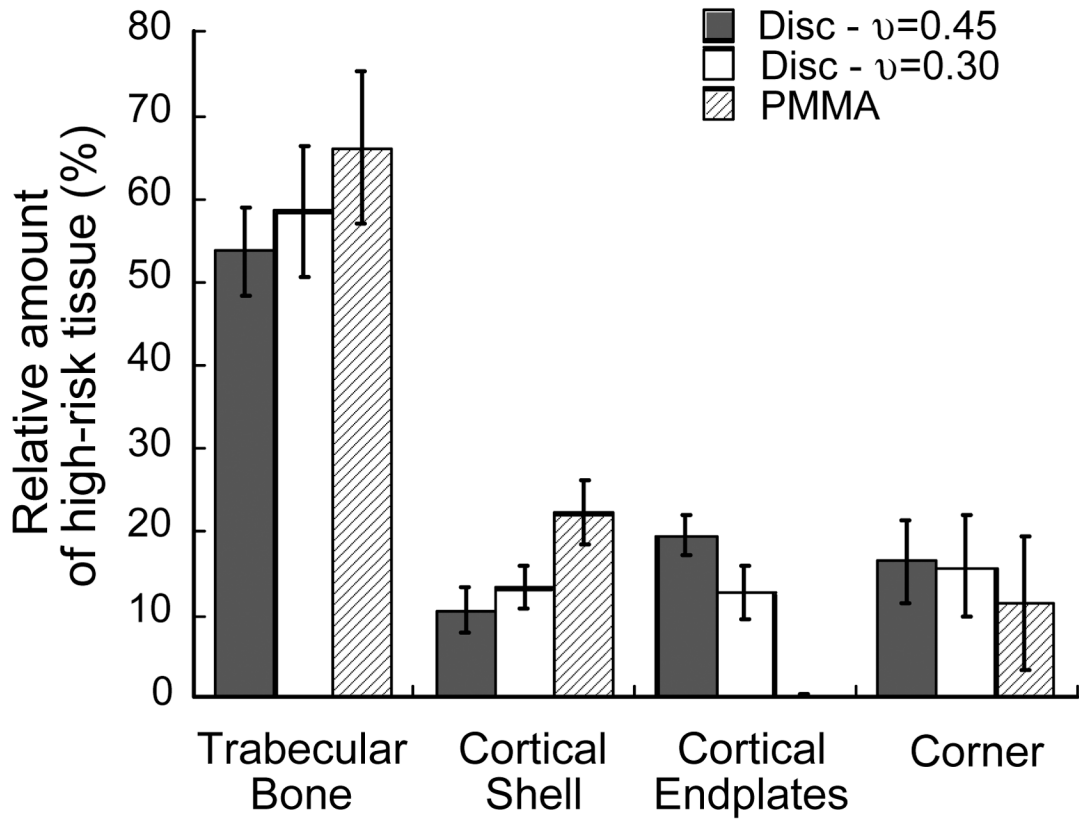


**Figure 5.** Comparison of the relative amount of high-risk tissue when the vertebral body was loaded to 1.0% apparent strain via a simulated disc or PMMA layer showing that loading through the PMMA layer resulted in minimal regions of high strain in the cortical endplates. A paired t-test was performed to compare the results for the disc with Poisson’s ratio of 0.30 and loading via PMMA to the baseline case (disc with Poisson’s ratio of 0.45). All comparisons were significantly different ( $p < 0.05$ ) except for the comparison of the relative amount of high-risk tissue in the corner regions when loading via the two simulated discs.

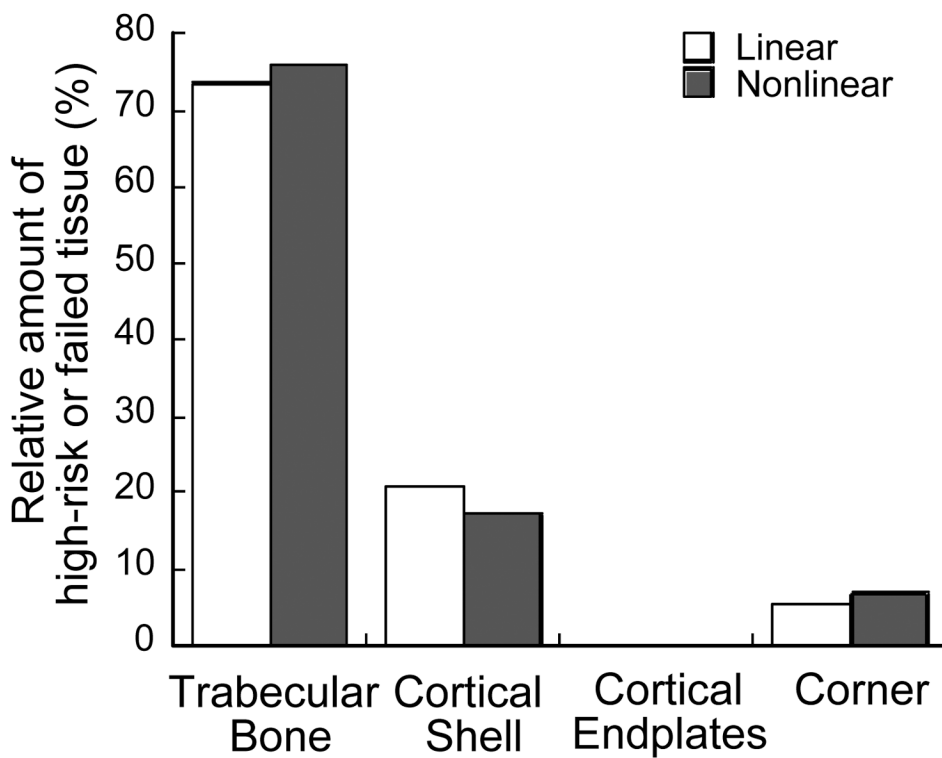


**Figure 6.** Comparison of the results from a linear and a fully nonlinear analysis for a single vertebra. The relative amount of high-risk tissue (linear) in the different units — trabecular bone, cortical shell, cortical endplates, and corner — compared well with the relative amount of failed tissue (nonlinear) determined at the apparent yield point of the whole vertebral body.

**Table 1**

Densitometric and morphologic parameters describing the vertebral bodies. The trabecular parameters were determined from a maximum size cuboid of trabecular bone that could be fit within the vertebral body, not including the shell or endplates. The average cortical shell thickness was determined in the region excluding the endplates [11].

Parameter	Mean $\pm$ S.D. (n=13)
BV/TV	0.096 $\pm$ 0.031
Tb. Th. (microns)	241 $\pm$ 23
Tb. Sp. (mm)	1.09 $\pm$ 0.14
SMI	1.59 $\pm$ 0.25
Avg. Shell Thickness (mm)	0.38 $\pm$ 0.06

**Table 2**

Maximum and minimum principal strain values for the thirteen specimens loaded to 1.0% apparent strain. Since the strains were not normally distributed, the median values and percentiles (25<sup>th</sup>, 75<sup>th</sup>, 90<sup>th</sup>) are shown.

Specimen No.	Principal Strains ( $\mu$ strain)	
	Minimum	Maximum
1	-140 (-80, -250, -430)	127 (67, 217, 347)
2	-193 (-103, -353, -533)	162 (102, 242, 362)
3	-212 (-122, -392, -692)	191 (101, 331, 511)
4	-143 (-83, -253, -413)	127 (67, 207, 317)
5	-141 (-81, -231, -331)	102 (72, 162, 242)
6	-192 (-102, -342, -582)	167 (97, 277, 437)
7	-128 (-58, -248, -428)	103 (53, 193, 323)
8	-103 (-63, -163, -223)	71 (51, 111, 151)
9	-184 (-104, -324, -494)	156 (96, 236, 346)
10	-169 (-99, -299, -479)	136 (76, 226, 336)
11	-159 (-89, -269, -429)	131 (81, 201, 291)
12	-173 (-93, -313, -533)	152 (82, 262, 432)
13	-182 (-102, -312, -472)	147 (87, 207, 287)